HHS Public Access

Author manuscript

Nat Cell Biol. Author manuscript; available in PMC 2013 August 18.

Published in final edited form as:

Nat Cell Biol. 2011 June ; 13(6): 660–667. doi:10.1038/ncb2231.

Protein Kinase A Governs a RhoA-RhoGDI Protrusion-Retraction Pacemaker in Migrating Cells

Eugene Tkachenko[1,4], **Mohsen Sabouri-Ghomi**[2], **Olivier Pertz**[3], **Chungho Kim**[1], **Edgar Gutierrez**[4], **Matthias Machacek**[2], **Alex Groisman**[4], **Gaudenz Danuser**[2,5], and **Mark H. Ginsberg**[1,6]

[1]Department of Medicine, University of California San Diego, 9500 Gilman Drive, Mail Code 0726, La Jolla, CA 92093 [2]Department of Cell Biology, The Scripps Research Institute, 10550 N. Torrey Pines Road, La Jolla, CA 92037 [3]Department of Biomedicine, University of Basel, Mattenstrasse 28, 4058 Basel, Switzerland [4]Department of Physics, University of California, San Diego, 9500 Gilman Drive, Mail Code 0374, La Jolla, CA, 92093

Abstract

The cyclical protrusion and retraction of the leading edge is a hallmark of many migrating cells involved in processes such as development, inflammation, and tumorigenesis. The molecular identity of signaling mechanisms that control these cycles has remained unknown. Here, we used live cell imaging of biosensors to monitor spontaneous morphodynamic and signaling activities, and employed correlative image analysis to examine the role of cAMP-activated Protein Kinase A (PKA) in protrusion regulation. PKA activity at the leading edge is closely synchronized with rapid protrusion and with the activity of RhoA. Ensuing PKA phosphorylation of RhoA and the resulting increased interaction between RhoA and RhoGDI establishes a negative feedback that controls the cycling of RhoA activity at the leading edge. Thus, cooperation between PKA, RhoA, and a RhoGDI forms a pacemaker that governs the morphodynamic behavior of migrating cells.

Keywords

Cell migration; cAMP activated Protein Kinase A; Rho GTPase; cell protrusion; RhoGDI

Cell movement requires precise spatiotemporal regulation of interconnected mechanical and biochemical signaling networks. Cytoskeletal remodeling at the front of a cell moving via the mesenchymal or collective modes of migration results in formation of morphologically distinct leading edge which exhibits cycles of protrusion and retraction[1–3]. Many elements

[6]To whom correspondence should be addressed: mhginsberg@ucsd.edu, Phone:1-858-822-6432.
[5]Present address: Department of Cell Biology, Harvard Medical School, 240 Longwood Ave, Boston, MA 02115

Author Contributions: ET conceived the project, performed experiments, analyzed data, and wrote the paper. MS-G, CK and MM analyzed data and wrote software. OP conceived experiments and provided critical reagents. AG and EG manufactured micro patterned substrates. GD conceived experiments, analyzed data, and edited the paper. MHG conceived experiments, analyzed data, and wrote the paper.

involved in the formation of cell protrusion such as actin assembly and adhesions exhibit a similar cyclic behavior[1,3–5]; however, the molecular identity of the pacemakers of protrusion-retraction cycles and the signaling pathways that govern their frequency remain obscure.

Cyclic AMP-dependent protein kinase A (PKA), a kinase that regulates diverse cellular activities, is activated at the leading edge of some cell types migrating *in vitro*[6,7], and inhibition of PKA inhibits cell migration[8–11]. PKA regulates axonal guidance *in vivo*[12], morphogenetic movements in Xenopus[13], and mutations of a PKA phosphorylation site in doublecortin is associated with X-linked lissencephaly, a neuronal migration defect in humans[14]. Furthermore, PKA facilitates the formation of peripheral ruffles[15,16] and influences protrusions at the leading edge of migrating CHO and smooth muscle cells[6,17]. PKA activity in the cell is compartmentalized; therefore information about spatiotemporal patterning of PKA activity is needed to understand the role of PKA in specific elements of cell migration and to identify relevant PKA substrates.

Here, we used live cell imaging of biosensors to monitor the spontaneous morphodynamic and signaling activities of renal epithelial PtK1 cells and human umbilical vein endothelial cells and employed correlative image analysis to examine the role of PKA in protrusion regulation with second-scale temporal and micron-scale spatial resolution. PKA inhibition led to reduced frequency of formation of protrusions of increased duration that propagated transversely along the cell edge. Furthermore, PKA activity at the leading edge exhibited close temporal and spatial correlation with the formation of protrusions and the activation of RhoA. This correlation depended on the phosphorylation of RhoA(Ser 188) by PKA, an event known to facilitate RhoA binding to RhoGDI [18], which leads to displacement of RhoA from the plasma membrane and precludes RhoA from interactions with downstream effectors[19–21]. Increased RhoGDI expression completely reversed the effects of PKA inhibition on protrusion morphodynamics, thus establishing that PKA governs the timing of protrusions by phosphorylation of RhoA resulting in RhoGDI-mediated termination of RhoA activity at the leading edge; hence the interaction of these three elements defines a pacemaker of the protrusion-retraction cycle. In consequence our studies provide direct mechanistic insight into how PKA, RhoA, and RhoGDI cooperate to control events at the leading edge of migrating cells.

Results

PKA controls protrusive duration, magnitude, and transverse propagation

To examine the effects of PKA activation at the leading edge of migrating cells on morphodynamic behaviors, we blocked PKA activity with a pseudosubstrate peptide, PKI[22,23] by transfecting PtK1 cells with cDNAs encoding PKI and enabled computer vision tracking of the membrane dynamics of the leading edge[2] with a membrane-localized GFP-CAAX (Fig.1a). We noted dramatically increased protrusion magnitude in PKI-expressing cells (Fig.1b; Movies 1, 2). To quantify these effects, we divided the cell edge into segments and followed their frame-to-frame displacements over time (SFigure 1)[2]. We then pasted the edge velocity values in each segment at one time-point of the movie into the column of a matrix and repeated the procedure time-point-by-time point over the entire movie. This

resulted in a cell-shape independent representation of protrusion and retraction dynamics as a morphodynamic map. Velocity values were color-coded from −50 nm/sec retraction (blue) to 50nm/sec protrusion (red) (Fig.1c). Confirming previous analyses of PtK1 cells [2], control cells revealed quasi-cyclical protrusion and retraction events for each segment of the cell edge. Importantly, the spatial autocorrelation of the protrusion and retraction activity along the cell edge had a full width at half maximum of 4.9 μm, [CI ±1.0] indicating that protrusion and retraction alternate on a length scale of single microns (see Methods).

As reported before [2], the transitions from retraction to protrusion propagated transversely along the cell edge, as indicated by a slanted streak of high forward velocity (arrow, Fig.1c). PKI transfection dramatically altered these dynamics. Over 50 min., much fewer protrusion-retraction cycles of much greater duration were observed (Fig.1c middle panel). Furthermore, PKA inhibition led to a more pronounced transversal protrusion propagation (arrow, Fig.1c middle panel). Representative segment edge velocity over time in a control or PKI-transfected cell is plotted in Fig.1c lower panel. Temporal auto-correlation function of the edge movement, averaged over all segments of the cell edge showed that inhibition of PKA activity prolonged the cycles from 130 to 820 sec (Fig.1d). Comparison of multiple cells (SFigure 1) confirmed a systematic, statistically significant increase of the cycle time [control (n=7) = 122±5.2(SEM) sec, and PKI (n=9) = 668±100.7 sec, P=0.0002]. Inhibition of PKA activity by 1μM KT-5720 or mislocalization of PKA by expression of mitochondrially-targeted AKAP peptide that binds all PKA (dual-AKAP trap) [24] resulted in protrusion morphodynamics similar to those observed with PKI transfection (SFigure2). These findings indicate that PKA regulates morphodynamics, controlling magnitude, duration, and transverse propagation of protrusions.

Temporal correlation of PKA activity with protrusion

We examined temporal and spatial correlations of PKA activity with protrusion using a membrane-bound FRET-based PKA biosensor (pmAKAR3) (SFigure3)[25]. CFP fluorescence tracked the leading edge (Fig.2a left) and YFP/CFP fluorescent emissions were analyzed by a MATLAB® program that corrects for dark current, variations in excitation light intensities, uneven field illumination, background autofluorescence, and rates of donor and acceptor photobleaching (see Methods) to calculate PKA activity FRET ratios (Fig.2a right). Protrusion velocity and FRET signals at different distances from the cell edge were collected (Fig.2b).

PKA activity within 1μm of the leading edge (Fig.2c) varied with a similar periodicity to protrusion-retraction (Fig.2d). Because the biosensor is a PKA substrate, at high expression levels, it could be a dominant-negative suppressor of PKA signaling. Accordingly, we selected cells with modest biosensor expression and verified that the duration of protrusion-retraction cycles was not altered(Fig.2e).

Temporal cross-correlations between FRET and edge velocity at different time lags were obtained in each sampling window (Fig.2b) by computing the Pearson's correlation coefficient between the collected time series. Mean correlation functions of the entire leading edge of the cell were obtained by averaging the correlation coefficient over all sampling windows for each temporal lag. Of note, averaging at the level of the correlation

coefficients permitted us to extract robust relationships between signaling and cell edge movement despite the spatially heterogeneous protrusion and retraction states of an individual cell. Integrating the data from 3 cells, we found a significant ($P<0.0001$) temporal cross-correlation of cell edge protrusions with PKA activity within 1μm from the cell edge (Fig.2f). The location of the cross-correlation maximum indicated a time shift of 22 sec, [CI ±13](CI - 95% Confidence Interval) between the peaks of PKA activity and protrusion velocity (Fig.2f), i.e. maximum activity is slightly delayed relative to fastest edge advancement. In primary Endothelial Cells peak PKA activity also slightly trailed maximal protrusion velocities (SFigure 3). PKA activity measured up to 4 μm from the cell edge maintained this temporal cross-correlation (Fig.2f). FRET data generated by a PKA-insensitive mutant biosensor generated insignificant, random correlation values at any time shift (SFigure 3). The tight temporal cross-correlation between PKA activity and edge movement suggested that they are causally-linked.

PKA Phosphorylation Regulates the Dynamics of RhoA Activation

We next sought PKA substrates that account for its linkage to morphodynamics. RhoA is a PKA substrate[18] and RhoA activity at the leading edge synchronizes with cell protrusion[26]. We used a single chain, RhoA biosensor to measure the RhoA activity[27] and we selected cells with moderate expression of the biosensor in which the timing of protrusions was similar to non-transfected cells (see Fig.3c). However, all cells that expressed the RhoA biosensor exhibited prolonged and less periodic protrusions (not shown). Modest expression biosensor of different design[28] did not affect morphodynamics and was used in all experiments reported here. These two biosensors differ in their mechanism of targeting plasma membrane; specifically the second biosensor contains the authentic RhoA C-terminus, thereby preserving its PKA phosphorylation and RhoGDI binding sites. These differences suggested the role of RhoA/RhoGDI interaction in control of protrusion morphodynamics by PKA phosphorylation of RhoA. All protrusion velocity and activity maps used for the analyses described below are in SFigure 4.

Temporal cross-correlation of RhoA activities and protrusion within 0.4 μm of the cell edge resembled the cross-correlation between PKA and protrusion (Fig.3a). This finding suggested that PKA and RhoA activities are causally-linked. Indeed, PKA phosphorylation of RhoA(Ser188) increases RhoA's affinity for RhoGDI reducing RhoA activity in part by sequestration from the membrane[18]. We therefore created a PKA-resistant RhoA(S188A) reporter and expressed at levels that did not alter the timing of protrusions (Fig.3c). As expected, activation of PKA resulted in increased binding of RhoGDI to RhoA but not RhoA(S188A) reporters (SFigure 4f). The activity of RhoA(S188A) exhibited a dramatically altered relationship with protrusions (Fig.3a). The most prominent feature of the cross-correlation between protrusion and the RhoA(S188A) activity was a negative peak 40 sec after peak velocity of protrusions (Fig.3a). Thus, PKA-mediated phosphorylation of RhoA at Ser 188 regulates the timing of RhoA activation at the leading edge.

As noted above, phosphorylation of RhoA increases its affinity for RhoGDI, leading us to suspect that mistiming of RhoA(S188A) activation was due to reduced affinity for RhoGDI. To test this idea, we over-expressed RhoGDI in cells expressing RhoA or RhoA(S188A)

activity reporters. In RhoGDI over-expressing cells, peaks of activities of wild type RhoA and RhoA(S188A) mutant occurred ~30 sec before protrusions reached maximal velocities (Fig.3b). We ascribe this leftward shift in the temporal correlation of RhoA and protrusive activity to early termination of RhoA signaling at the plasma membrane in RhoGDI-over expressing cells. Early termination of RhoA activity by over-expression of RhoGDI reduced the average duration of protrusion cycle from 122 sec, [CI ±5.2] to 92 sec, [CI ±6.5]. Thus, inhibition of PKA-mediated phosphorylation of RhoA alters the relationship between protrusions and RhoA activity by reducing the affinity of RhoA for RhoGDI, whereas over-expression of RhoGDI compensates for this reduced affinity.

Over-expression of RhoA(S188A) or RhoA phenocopies the effects of PKA inhibition on protrusion dynamics

As noted above, inhibition of PKA resulted in increased duration, magnitude, and transverse propagation of protrusions. We hypothesized that this was due to the loss of RhoA phosphorylation, resulting in prolonged and elevated RhoA signaling at the plasma membrane. To test this idea, we over-expressed RhoA(S188A) which resulted in morphodynamics resembling those observed with inhibition of PKA, i.e. these cells showed a marked reduction in the frequency and an increase in the duration and transverse propagation of protrusions (Fig.4; SFigure 5). Moreover, this phenotype was due to reduced regulation by RhoGDI, because co-expression of RhoGDI with RhoA(S188A) resulted in reversal of all the temporal effects of RhoA(S188A) expression, including shortening of duration and reduction in transverse propagation of protrusions (Fig.4; SFigure 5). The increased amplitude of protrusions and retractions remaining after co-expression of RhoGDI and RhoA(S188A) is ascribed to an overall increase in RhoA. Over-expression of wild type RhoA with and without RhoGDI resulted in cell phenotypes similar to the described above for RhoA(S188A) with and without RhoGDI (SFigure 6) confirming the importance of the ratio of RhoA/RhoGDI in the timing of protrusions.

The foregoing data suggested that the interaction of RhoA with RhoGDI led to the termination of protrusions. A recent study reported that, in some cells, over-expression of Rho GTPases results in degradation of endogenous RhoGTPases due to competition for RhoGDIs[29]. We did not observe a reduction in protein levels of Rac1 or CDC42 in cells over-expressing wild type RhoA or RhoA(S188A) alone or in combination with RhoGDI1 (SFigure 6d). We therefore reasoned that over-expression of a RhoA mutant that does not interact with RhoGDI and incapable of sequestering it to reduce protein levels of endogenous RhoGTPases[29] should also increase the duration of protrusions, and that over-expression of RhoGDI should not correct the increased protrusion duration. Over-expression of RhoA(R68E), which is defective in binding RhoGDI [30], led to a dramatic increase in the amplitude and duration of protrusions. In sharp contrast to the phenotype caused by wild type RhoA or RhoA(S188A), over-expression of RhoGDI did not significantly alter the morphodynamics of protrusions caused by RhoA(R68E)(Fig.5; SFigure 7). Thus, the effect of RhoGDI on morphodynamics reported here depends on its ability to directly bind to RhoA.

Over-expression of RhoGDI reverses the effect of PKA inhibition on protrusion morphodynamics

PKA has many potential substrates that could be involved in the control of morphodynamics of protrusions. The foregoing experiments showed that PKA controls the timing of RhoA activity by phosphorylation of Ser188, and that this effect depends on the RhoGDI-RhoA interaction. To assess whether PKA modulation of RhoGDI-RhoA interaction is a master regulator of the duration and transverse propagation of protrusions we inhibited PKA with PKI and simultaneously over-expressed RhoGDI (SFigure 8). Over-expression of RhoGDI reversed the effect of PKA inhibition (Fig.6a; SFigure 8). Specifically, protrusion duration (Fig.6b,c) and their transverse propagation (Fig.6a) resembled control cells. Thus, PKA phosphorylation of RhoA and its resulting effects on RhoGDI-RhoA interaction control the cycling of functional RhoA activity, and thus protrusion-retraction cycles.

Adhesion-dependent activation of PKA during protrusions

As shown above, PKA shortens cell protrusions by increasing the affinity of RhoA for RhoGDI through RhoA phosphorylation. We next wished to ask whether protrusion might activate PKA, thereby initiating a self-inhibitory feedback mechanism. Disrupting actin filaments with latrunculin A or antibody blockade of integrins inhibits leading edge PKA activation[6]; however, integrin blockade also inhibited protrusion. To directly test the role of adhesion as a requirement for PKA activation, we examined zones in which adhesion was blocked yet passive protrusion was maintained. We produced micropatterned substrates comprised of alternating 16 μm wide fibronectin stripes and 16μm inert polylysine-polyethylene glycol (PLL-PEG) stripes of (Fig.7a, left). Cells plated extended lamellipodia along the fibronectin stripes (Fig.7a middle; Movie 3) and tips of these lamellipodia had high level of PKA activity in the fibronectin-adherent regions (Fig.7a, right). The morphodynamic maps (Fig.7b) revealed cycles of similar duration in adherent and non-adherent zones and those in the non-adherent zone were spatially connected to those in the adherent zone (black arrows, Fig.7b, top panel) suggesting that that edge movements in non-adherent zones were passive extensions of those generated in adherent zones. In spite of ongoing protrusions, the cell edge in the non-adherent PLL-PEG coated strips was virtually devoid of PKA activity (Fig.7b, lower panel). Thus, the combination of protrusion and adhesion of the leading edge results in PKA activation, thereby explaining the occurrence of maximal PKA activity shortly after peak protrusion velocity (Fig.2f).

Discussion

Many motile cells pathfind by cycling between protrusion and retraction of the leading edge. We found that in PtK1 epithelial cells a single protrusion-retraction-protrusion cycle lasts ~80 s and spans a segment of the leading edge of about 5μm. To understand these highly localized morphodynamics, we examined the intersecting roles of PKA, RhoA and RhoGDI in the regulation of constitutively-migrating epithelial cells, and endothelial cells. Our experiments re-emphasize that transient and highly localized increases in RhoA activity are associated with protrusion[28,31]. Here, we report that the close association of RhoA activity with protrusion requires phosphorylation of RhoA(Ser 188) by PKA. This is evidenced by: First, inhibition of PKA decreased frequency and increased the duration of protrusions

formed at the leading edge. Second, PKA activity closely temporally correlated with both RhoA activity and edge advancement. Thirdly, correlation of protrusion and RhoA activity was altered in non-phosphorylatable RhoA(S188A). Phosphorylation of RhoA increases its affinity for RhoGDI[18], leading to displacement of RhoA from the plasma membrane[19,21] and inhibition of effectors interactions. Over-expression of RhoGDI corrected the mistiming of RhoA(S188A) activation. Fourth, over-expression of RhoGDI corrected the effects of over expression of RhoA and RhoA(S188A) but not that of RhoA(R68E), a mutant which can not bind to RhoGDI[30], on the timing of the protrusion-retraction cycle. Fifth, increased RhoGDI expression also overcame the effects of blocking PKA activity on protrusion morphodynamics. Together, these data show that the cycling of active RhoA at the plasma membrane controls the pace of the protrusion-retraction cycles. RhoA may control protrusion by promotion of actin nucleation through formins [32]. Alternatively, collisions of transversely propagated protrusions lead to their termination and plays critical rode in determining their duration[2]. Therefore, by reducing the frequency of new protrusions, RhoA may prevent lateral inhibition, thereby resulting in protrusions of greater duration, amplitude and transverse propagation. In either case, here we, identify PKA activity, in particular its effect on RhoA- RhoGDI interaction by phosphorylating RhoA(Ser188), as a pacemaker of the protrusion-retraction cycle (Fig.7c).

PKA is activated at the leading edge of migrating cells[6,7,17] and PKA inhibition reduces the number of protrusions formed at the leading edge[6]. In accord with those observations, we found that blocking PKA activity markedly widened the length-scale of protrusions while increasing their duration. This suggested that PKA activity limits a protrusion-promoting signal both in time and space. We propose that protrusion mechanically activates PKA via adhesion-mediated mechano-transduction, placing PKA in the core of a self-inhibiting feedback loop between RhoA and protrusion (Fig.7c). Mechanistically, this PKA activation may be induced by increasing tractional forces during protrusion events. In PtK1 cells traction force maxima lag behind the maximal protrusive velocity by ∼20 sec [3]. In remarkable agreement with this timing, our data here show that the activation of PKA was also slightly delayed relative to the protrusion velocity. Thus, we find that the linked activities of integrins, PKA, and RhoA(Ser 188)-phosphorylation establishes a mechano-responsive governor of the protrusion-retraction cycle.

Alternative mechanisms by which PKA could inhibit RhoA, include inhibition of Giα12,13 signaling[33] or inhibiting RhoGEF(s) function[34,35]. However, our data strongly favor direct phosphorylation on RhoA here. Specifically, mutating the PKA phosphorylation site in RhoA(S188A) leads to loss of positive correlation between protrusion and RhoA activity. RhoA phosphorylation could change its affinity for specific effectors[36] or its lateral translocation into different membrane microdomains[37] instead of affecting the interaction between RhoA and RhoGDI. However, these mechanisms would not readily explain the dramatic complementation by RhoGDI over-expression. Similarly, the finding that RhoGDI over-expression reversed all of the effects of PKA inhibition provides a compelling argument that the effects of PKA inhibition on morphodynamics is due to phosphorylation of RhoA and resulting increased affinity for RhoGDI. Therefore, direct phosphorylation by PKA controls RhoA activity cycles that regulate protrusion at the leading edge.

Previous studies suggested that that RhoGDI, along with GTPase activating proteins (GAPs) and GDP/GTP exchange factors (GEFs), plays an active role in Rho GTPase turnover in cellular protrusions[38]. Our studies provide demonstrate that RhoA cycling regulated by PKA and RhoGDI is a part of protrusion-retraction pacemaker (Fig.7c). Therefore, the level of RhoGDI expression could set the gain function by which cell protrusive behavior responds to PKA activity as influenced, among other factors, by extracellular matrix composition[6,39] and substrate stiffness[40]. Hence, changes in RhoGDI expression might result in enhanced cellular migration on substrates characterized by otherwise suboptimal mechanical or chemical composition properties[41], helping to explain the role RhoGDI plays in determining the invasive and metastatic properties of cancers[42–44].

Methods

Constructs

Plasma membrane targeted PKA reporter AKAR3 (pmAKAR3) and RhoA activity reporter were previously described[25,28]. pcDNA3.1 (Invitrogen, Carlsbad, CA) encoding human RhoA fused to 3 tandem hemagglutinin (HA) tags was obtained from Missouri S&T cDNA Resource Center (Rolla, MO). Mutagenesis of RhoA Ser188 was done using the Quick Change mutagenesis kit (Stratagene, La Jolla, CA) according to manufacturer's protocol. pEFBos myc RhoGDI was a obtained from Martin Schwartz (University of Virginia)[45]. cDNAs encoding HA-tagged PKI in pcDNA 3.1 were gifts from Susan Taylor. H2b-EGFP in SIN18.hPGK.eGFP.WPRE was a gift from Jeffrey H. Price[46]. Mitochondrial membrane-targeted dual (RI&RII) AKAP peptide (AKAP trap) was previously described [24]. eGFP-RhoGDI construct in pcDNA3.1(Invitrogen) and RhoA R68E construct in PRK5M-cMyc vector were gifts from Celine DerMardirossian (The Scripps Research Institute, La Jolla).

Construction of mCherry-PKI in pcDNA 3.1

283 bp sequence encoding HA-PKI was amplified by PCR using primers that introduced ClaI and NotI sites at the N- and C-terminus, respectively, and ligated into corresponding sites of a pcDNA3.1 construct encoding mCherry[47] at the N-terminus and. The resulting open reading frame encodes mCherry-HA-PKI. *GFP-CAAX- in eGFP-N1* (Clontech, Mountain View, CA) was generated by inserting synthesized double strained DNA encoding K-Ras CAAX box into XhoI and BamHI cloning sites. mCherry-CAAX was generated by exchanging eGFP in eGFP-CAAX construct with mCherry using XhoI and BamHI sites.

Cell Culture

Female Rat Kangaroo Kidney Epithelial Cells (PtK1) cells were a gift from Clare Waterman (The National Heart, Lung, and Blood Institute). Cells were cultured in humidified incubator at 37°C, 5% CO2 in K-12 media (Invitrogen) containing 10% FBS and Penicillin/ Streptavidin (Invitrogen). For imaging, 25 mm glass coverslips (VistaVision No.1(VWR) were coated with 10 μg/ml human fibronectin (Dow Corning, Midland, MI) at RT for 1h and blocked with 1% heat-denatured bovine serum albumin (BSA) for 30 min. Cells were cultured on cover slips for 24 hr before experiments.

PTK1 cells were transduced with retrovirus encoding RhoA or RhoA(S188A) activity reporters. Retroviral production and transduction was done as previously described [28]. Transient transfections were performed using Amaxa nucleoporator (Lonza). 1×10^6 cells were resuspended in 100μl solution "R" containing 1–5 μg of plasmid construct and electroporated using program T-20. For experiments involving over-expression of RhoGDI in cells stably expressing RhoA or RhoA(S188A) reporter, cells were co-transfected by electroporation with RhoGDI and H2B-eGFP construct at ratio 4:1. H2B-eGFP labels only the nucleus, indicating transfected cells, and does not interfere with FRET imaging of the cell edge. For experiments involving over-expression of RhoA(wt, S188A or R68E), cells were transiently co-transfected with EGFP-CAAX , RhoA(wt, S188A or R68E) and either empty vector or RhoGDI at ratio (0.5:1:4). For experiments involving expression of PKI, cells were co transfected with EGFP-CAAX, PKI-cherry and empty vector or RhoGDI at ratio 0.5:1:4. Cells with high levels of mCherry expression were used for analysis. Immunostaining for phosphorylated PKA substrates was done to confirm an effect of PKI as previously described [48]. For all co-transfection combinations the levels of expression of RhoGDI and RhoA(wt, S188A or R68E) were checked by immunoblot analysis or by fluorescence of eGFP-fused form of RhoGDI.

Co-Immunoprecipitation and Immunoblot Analysis

Anti-GFP antibodies (Rosh) at concentration 2μg/ml and protein G sepharose beads (Invitrogen) were used for co-immunoprecipitation assay. Anti-HA antibodies 16B12 were obtained from Covance (Princeton, NJ). Anti- c-myc antibodies 9E10 were from Santa Cruz Biotechnology (Santa Cruz, CA). Anti-CDC42 and anti-RhoA antibodies were from Cell Signaling (Beverly MA). Anti-Rac1 antibodies were from Millipore (Billerica, MA). All antibodies were used for western blot analysis at dilution 1:1000.

Microscopy

Cells grown on cover glasses were mounted into CM-R-Z004 chamber (Live Cell Instrument, Inc., Seoul, Korea). The environmentally controlled microscopy system and FRET acquisition were previously described[6]. Time-lapse images were acquired for every 10 seconds with Plan-Apo 60x/1.4 numerical aperture (NA) oil emersion objective (Nikon).

Micro-patterning of fibronectin on glass coverslips

Fibronectin was labeled with AnaTaq HiLyte Fluor 647 protein labeling kit (AnaSpec, Fremont, CA) according to manufacturer's protocol. We fabricated polydimethylsiloxane (PDMS) stamps with 16 μm stripes spaced 16μm apart [49] and used these stamps to print a micropatterned fluorescent fibronectin substrate as described [50]. The nonprinted 16μm intervening stripes were back-filled with poly-L-lysine-polyethylene glycol (PLL-PEG), which renders them resistant to cell adhesion, by incubation of patterned coverslips for 30 min in PBS pH 7.4 solution of 0.5mg/ml of PLL-PEG ($mPEG_{1k}$-b-$PLKC_{100}$, Alamanda Polymers, Hunsville, AL).

Image processing

Time lapse series were edited in ImageJ (NIH, Bethesda, MD). Figures were assembled in Photoshop CS2, Illustrator CS2 and InDesign CS2 (Adobe Systems, Mountain View, CA). For all other image processing we used home-written Matlab functions (MathWorks, Natick, MA).

FRET analysis

Processing of FRET data was done using automated custom-built Matlab software. Our program subtracts dark current from raw images followed by correction for light source intensity fluctuations, uneven illumination of the field, background autofluorescence, variations in concentration of biosensor within a cell[51], and different rates of photobleaching for donor and acceptor fluorophores[52].

Cell edge tracking

Cell edges were detected via an intensity-based segmentation of images with membrane-bound fluorophor. The edge evolution in time was tracked computationally as described in[2]. Rates of protrusion and retraction (velocity maps) were calculated by finite differences of positions in consecutive frame triplets at T−1, T, and T+1 (SFigure 1).

Cross-Correlation analysis

Temporal cross-correlations between FRET signal and protrusion (edge velocity) windows at different lags were obtained in each sampling window (SFigure 1) by computing the Pearson's correlation coefficient. The correlation for the entire leading edge of the cell was obtained by averaging the correlation coefficient over all sampling windows for each temporal lag. To investigate the cell-to-cell heterogeneity of the cross-correlation between two activities, a common cross-correlation function was estimated by computing a smoothing spline for the ensemble of average cross-correlation data from different cells. The variance of the smoothing spline approximation and hence of the location of the maximum correlation was calculated by a non-parametric bootstrap method[53]. In this method the residuals of the approximated spline 2000 bootstrap samples were taken to reconstruct 2000 cross-correlation samples. From this sample pool, local variation of the spline around mean, variation in maximum correlation coefficient, and variation in location of the maximum correlation (time lag) were inferred. The 95% confidence interval for the estimated common cross-correlation was obtained in each location as the interval containing 95% of the bootstrapped spline samples.

Temporal auto-correlation of protrusions/retractions was computed by cross-correlation of edge velocity with itself. To analyze the difference in the duration of protrusions/retractions we measured the peak width in the autocorrelation plot at an arbitrarily chosen correlation value of 0.2.

Protrusion and retraction length scale evaluation

Protrusions and retraction length scale is the distance along the edge of the cell over which protrusion and retraction events become statistically independent from each other. Edge

movements are defined as independent when the spatial auto-correlation level of leading edge movements falls below 50% of its maximum value. For each cell, the spatial auto-correlation of edge movements where obtained by time-averaging the Pearson correlation coefficient at different spatial lags along the edge over the entire duration of the movie. A characteristic spatial auto-correlation of edge movements was calculated by fitting a smoothing spline to the ensemble of the auto-correlation data from different cells. The characteristic protrusion and retraction length scale was calculated from the full width at half maximum (FWHM) of the characteristic spatial auto-correlation curve.

Statistical analysis

Averages and SEMs were calculated and are shown in the graphs. Respective n values are shown in the figure legends. The indicated P values were obtained with two-tailed Student's t-tests.

Supplementary Material

Refer to Web version on PubMed Central for supplementary material.

Acknowledgements

Supported by Grants from the NIH (AR27214(MHG), HL31950(MHG), GM071868 (GD), F32 HL094012-01 (E.T.) and the Cell Migration Consortium(MHG,GD).

References

1. Giannone G, et al. Periodic lamellipodial contractions correlate with rearward actin waves. Cell. 2004; 116:431–443. [PubMed: 15016377]
2. Machacek M, Danuser G. Morphodynamic profiling of protrusion phenotypes. Biophys J. 2006; 90:1439–1452. [PubMed: 16326902]
3. Ji L, Lim J, Danuser G. Fluctuations of intracellular forces during cell protrusion. Nat Cell Biol. 2008; 10:1393–1400. [PubMed: 19011623]
4. Giannone G, et al. Lamellipodial actin mechanically links myosin activity with adhesion-site formation. Cell. 2007; 128:561–575. [PubMed: 17289574]
5. Ponti A, Machacek M, Gupton SL, Waterman-Storer CM, Danuser G. Two distinct actin networks drive the protrusion of migrating cells. Science. 2004; 305:1782–1786. [PubMed: 15375270]
6. Lim CJ, et al. Integrin-mediated protein kinase A activation at the leading edge of migrating cells. Mol Biol Cell. 2008; 19:4930–4941. [PubMed: 18784251]
7. Paulucci-Holthauzen AA, et al. Spatial distribution of protein kinase A activity during cell migration is mediated by A-kinase anchoring protein AKAP Lbc. J Biol Chem. 2009; 284:5956–5967. [PubMed: 19106088]
8. Edin ML, Howe AK, Juliano RL. Inhibition of PKA blocks fibroblast migration in response to growth factors. Exp Cell Res. 2001; 270:214–222. [PubMed: 11640885]
9. Goldfinger LE, Han J, Kiosses WB, Howe AK, Ginsberg MH. Spatial restriction of alpha4 integrin phosphorylation regulates lamellipodial stability and alpha4beta1-dependent cell migration. J Cell Biol. 2003; 162:731–741. [PubMed: 12913113]
10. Howe AK, Baldor LC, Hogan BP. Spatial regulation of the cAMP-dependent protein kinase during chemotactic cell migration. Proc Natl Acad Sci U S A. 2005; 102:14320–14325. [PubMed: 16176981]
11. O'Connor KL, Shaw LM, Mercurio AM. Release of cAMP gating by the alpha6beta4 integrin stimulates lamellae formation and the chemotactic migration of invasive carcinoma cells. J Cell Biol. 1998; 143:1749–1760. [PubMed: 9852165]

12. Murray AJ, Tucker SJ, Shewan DA. cAMP-dependent axon guidance is distinctly regulated by Epac and protein kinase A. J Neurosci. 2009; 29:15434–15444. [PubMed: 20007468]
13. Song BH, Choi SC, Han JK. Local activation of protein kinase A inhibits morphogenetic movements during Xenopus gastrulation. Dev Dyn. 2003; 227:91–103. [PubMed: 12701102]
14. Schaar BT, Kinoshita K, McConnell SK. Doublecortin microtubule affinity is regulated by a balance of kinase and phosphatase activity at the leading edge of migrating neurons. Neuron. 2004; 41:203–213. [PubMed: 14741102]
15. Deming PB, Campbell SL, Baldor LC, Howe AK. Protein kinase A regulates 3-phosphatidylinositide dynamics during platelet-derived growth factor-induced membrane ruffling and chemotaxis. J Biol Chem. 2008; 283:35199–35211. [PubMed: 18936099]
16. O'Connor KL, Nguyen BK, Mercurio AM. RhoA function in lamellae formation and migration is regulated by the alpha6beta4 integrin and cAMP metabolism. J Cell Biol. 2000; 148:253–258. [PubMed: 10648558]
17. Howe AK. Regulation of actin-based cell migration by cAMP/PKA. Biochim Biophys Acta. 2004; 1692:159–174. [PubMed: 15246685]
18. Lang P, et al. Protein kinase A phosphorylation of RhoA mediates the morphological and functional effects of cyclic AMP in cytotoxic lymphocytes. Embo J. 1996; 15:510–519. [PubMed: 8599934]
19. DerMardirossian C, Bokoch GM. GDIs: central regulatory molecules in Rho GTPase activation. Trends Cell Biol. 2005; 15:356–363. [PubMed: 15921909]
20. DerMardirossian C, Rocklin G, Seo JY, Bokoch GM. Phosphorylation of RhoGDI by Src regulates Rho GTPase binding and cytosol-membrane cycling. Mol Biol Cell. 2006; 17:4760–4768. [PubMed: 16943322]
21. Ueda T, Kikuchi A, Ohga N, Yamamoto J, Takai Y. Purification and characterization from bovine brain cytosol of a novel regulatory protein inhibiting the dissociation of GDP from and the subsequent binding of GTP to rhoB p20, a ras p21-like GTP-binding protein. J Biol Chem. 1990; 265:9373–9380. [PubMed: 2111820]
22. Knighton DR, et al. Structure of a peptide inhibitor bound to the catalytic subunit of cyclic adenosine monophosphate-dependent protein kinase. Science. 1991; 253:414–420. [PubMed: 1862343]
23. Taylor SS, et al. Dynamics of signaling by PKA. Biochim Biophys Acta. 2005; 1754:25–37. [PubMed: 16214430]
24. Burns-Hamuro LL, et al. Designing isoform-specific peptide disruptors of protein kinase A localization. Proc Natl Acad Sci U S A. 2003; 100:4072–4077. [PubMed: 12646696]
25. Allen MD, Zhang J. Subcellular dynamics of protein kinase A activity visualized by FRET-based reporters. Biochem Biophys Res Commun. 2006; 348:716–721. [PubMed: 16895723]
26. Machacek M, et al. Coordination of Rho GTPase activities during cell protrusion. Nature. 2009
27. Nakamura T, Aoki K, Matsuda M. Monitoring spatio-temporal regulation of Ras and Rho GTPase with GFP-based FRET probes. Methods. 2005; 37:146–153. [PubMed: 16288890]
28. Pertz O, Hodgson L, Klemke RL, Hahn KM. Spatiotemporal dynamics of RhoA activity in migrating cells. Nature. 2006; 440:1069–1072. [PubMed: 16547516]
29. Boulter E, et al. Regulation of Rho GTPase crosstalk, degradation and activity by RhoGDI1. Nat Cell Biol. 2010; 12:477–483. [PubMed: 20400958]
30. Ho TT, Merajver SD, Lapiere CM, Nusgens BV, Deroanne CF. RhoA-GDP regulates RhoB protein stability Potential involvement of RhoGDIalpha. J Biol Chem. 2008; 283:21588–21598. [PubMed: 18524772]
31. Machacek M, et al. Coordination of Rho GTPase activities during cell protrusion. Nature. 2009; 461:99–103. [PubMed: 19693013]
32. Ridley AJ. Rho GTPases and actin dynamics in membrane protrusions and vesicle trafficking. Trends Cell Biol. 2006; 16:522–529. [PubMed: 16949823]
33. Manganello JM, Huang JS, Kozasa T, Voyno-Yasenetskaya TA, Le Breton GC. Protein kinase A-mediated phosphorylation of the Galpha13 switch I region alters the Galphabetagamma13-G protein-coupled receptor complex and inhibits Rho activation. J Biol Chem. 2003; 278:124–130. [PubMed: 12399457]

34. Diviani D, Baisamy L, Appert-Collin A. AKAP-Lbc: a molecular scaffold for the integration of cyclic AMP and Rho transduction pathways. Eur J Cell Biol. 2006; 85:603–610. [PubMed: 16460837]
35. Laudanna C, Campbell JJ, Butcher EC. Elevation of intracellular cAMP inhibits RhoA activation and integrin-dependent leukocyte adhesion induced by chemoattractants. J Biol Chem. 1997; 272:24141–24144. [PubMed: 9305861]
36. Nusser N, et al. Serine phosphorylation differentially affects RhoA binding to effectors: implications to NGF-induced neurite outgrowth. Cell Signal. 2006; 18:704–714. [PubMed: 16109481]
37. Hancock JF. Lipid rafts: contentious only from simplistic standpoints. Nat Rev Mol Cell Biol. 2006; 7:456–462. [PubMed: 16625153]
38. Dransart E, Morin A, Cherfils J, Olofsson B. RhoGDI-3, a promising system to investigate the regulatory function of rhoGDIs: uncoupling of inhibitory and shuttling functions of rhoGDIs. Biochem Soc Trans. 2005; 33:623–626. [PubMed: 16042558]
39. Gonzalez AM, Claiborne J, Jones JC. Integrin cross-talk in endothelial cells is regulated by protein kinase A and protein phosphatase 1. J Biol Chem. 2008; 283:31849–31860. [PubMed: 18806263]
40. Lavandero S, et al. Changes in cyclic AMP dependent protein kinase and active stiffness in the rat volume overload model of heart hypertrophy. Cardiovasc Res. 1993; 27:1634–1638. [PubMed: 8287442]
41. Gupton SL, Waterman-Storer CM. Spatiotemporal feedback between actomyosin and focal-adhesion systems optimizes rapid cell migration. Cell. 2006; 125:1361–1374. [PubMed: 16814721]
42. Gildea JJ, et al. RhoGDI2 is an invasion and metastasis suppressor gene in human cancer. Cancer Res. 2002; 62:6418–6423. [PubMed: 12438227]
43. Wu W, Graves LM, Gill GN, Parsons SJ, Samet JM. Src-dependent phosphorylation of the epidermal growth factor receptor on tyrosine 845 is required for zinc-induced Ras activation. J Biol Chem. 2002; 277:24252–24257. [PubMed: 11983694]
44. Zhao L, Wang H, Li J, Liu Y, Ding Y. Overexpression of Rho GDP-dissociation inhibitor alpha is associated with tumor progression and poor prognosis of colorectal cancer. J Proteome Res. 2008; 7:3994–4003. [PubMed: 18651761]
45. Fukumoto Y, et al. Molecular cloning and characterization of a novel type of regulatory protein (GDI) for the rho proteins, ras p21-like small GTP-binding proteins. Oncogene. 1990; 5:1321–1328. [PubMed: 2120668]
46. Kita-Matsuo H, et al. Lentiviral vectors and protocols for creation of stable hESC lines for fluorescent tracking and drug resistance selection of cardiomyocytes. *PLoS ONE*. 2009; 4:5046.
47. Shu X, Shaner NC, Yarbrough CA, Tsien RY, Remington SJ. Novel chromophores and buried charges control color in mFruits. Biochemistry. 2006; 45:9639–9647. [PubMed: 16893165]
48. Lim CJ, et al. Alpha4 integrins are type I cAMP-dependent protein kinase-anchoring proteins. Nat Cell Biol. 2007; 9:415–421. [PubMed: 17369818]
49. Tkachenko E, Gutierrez E, Ginsberg MH, Groisman A. An easy to assemble microfluidic perfusion device with a magnetic clamp. Lab Chip. 2009; 9:1085–1095. [PubMed: 19350090]
50. Thery M, Piel M. Adhesive micropatterns for cells: a microcontact printing protocol. CSH Protoc 2009. 2009 pdb prot5255.
51. Nakamura, T.; Kurokawa, K.; Kiyokawa, E.; Matsuda, M.; William, E.; Balch, C.J. D. a. A. H. Methods in Enzymology. Vol. 406. Academic Press; 2006. p. 315
52. Hodgson L, Nalbant P, Shen F, Hahn K. Imaging and photobleach correction of Mero-CBD, sensor of endogenous Cdc42 activation. Methods Enzymol. 2006; 406:140–156. [PubMed: 16472656]
53. Efron B, Tibshirani R. An Introduction to the bootstrap. (Chapman & Hall, 1993).

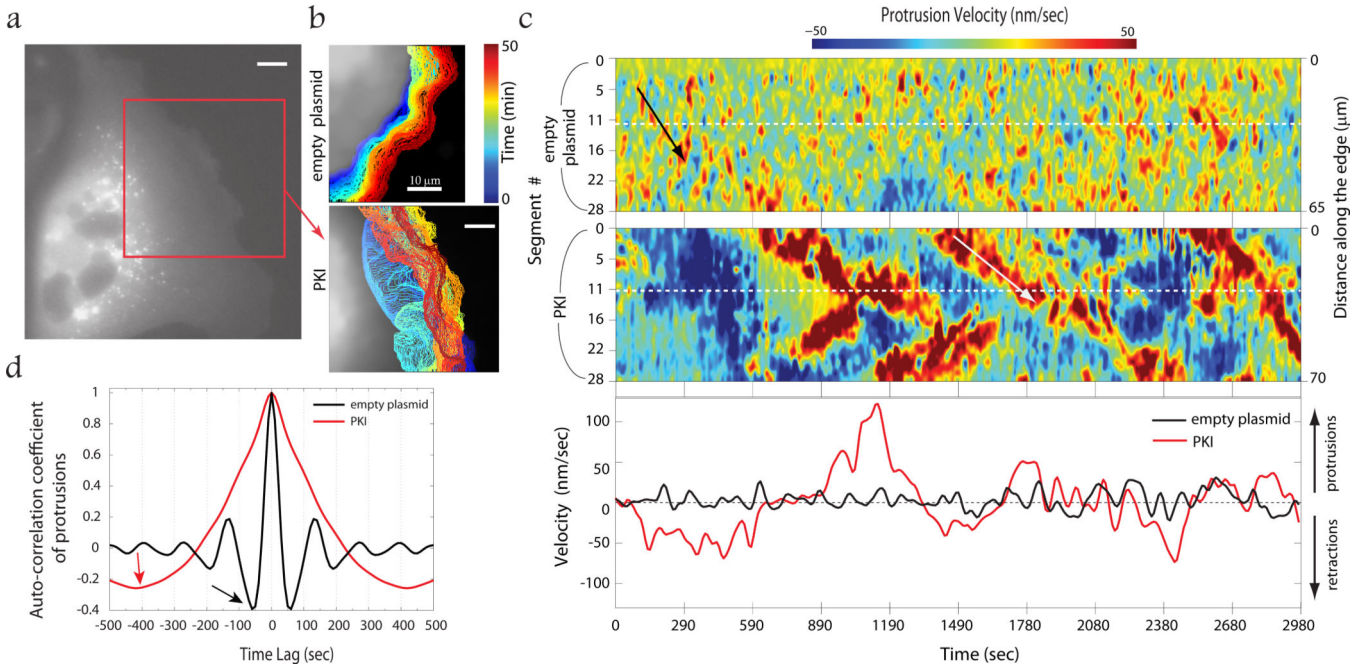

Figure 1. PKA controls the characteristic time and magnitude of protrusive activity

a) PtK1 cell transfected with cDNA encoding membrane targeted GFP-CAAX was visualized by fluorescence microcopy and the localization of the GFP was used to define the cell edge; the multiple intracellular vesicular structures presumably contain newly-synthesized GFP-CAAX en route to the plasma membrane. Cell transfected with mCherry-PKI were identifie d by mCherry fluorescence. The red box indicates the region analyzed in the PKI-expressing cell in (b). Scale bar is 10 μm. b) Contours of the leading edges of two cells from series of images taken with 10 sec intervals over 50 min, with the color of the contour showing the time when the image was taken. c) Velocity maps of the protrusions along the cell leading edge, as evaluated from the evolution from the edge contours in (b). In the two upper panels, the abscissa indicates time, the ordinate indicates the position along the edge in terms of the segment number (left) and the absolute distance (right), and the color-coding of the diagram shows the local edge protrusion velocity ranging from −50 (blue) to 50 (red) nm/sec. Oblique arrows (black and white) indicate transverse waves of protrusion propagating along the cell edge. The bottom panel is a plot of the edge velocity of the segments marked by the white dashed lines in the two upper panels. Similar maps were observed for mono and multi-nucleate PTK1 cells. d) Temporal auto-correlation of protrusion velocities. In control cell, protrusion and retraction events repeat every 130 sec (black arrow). Expression of PKI resulted in cycles of 820 sec (red arrow).

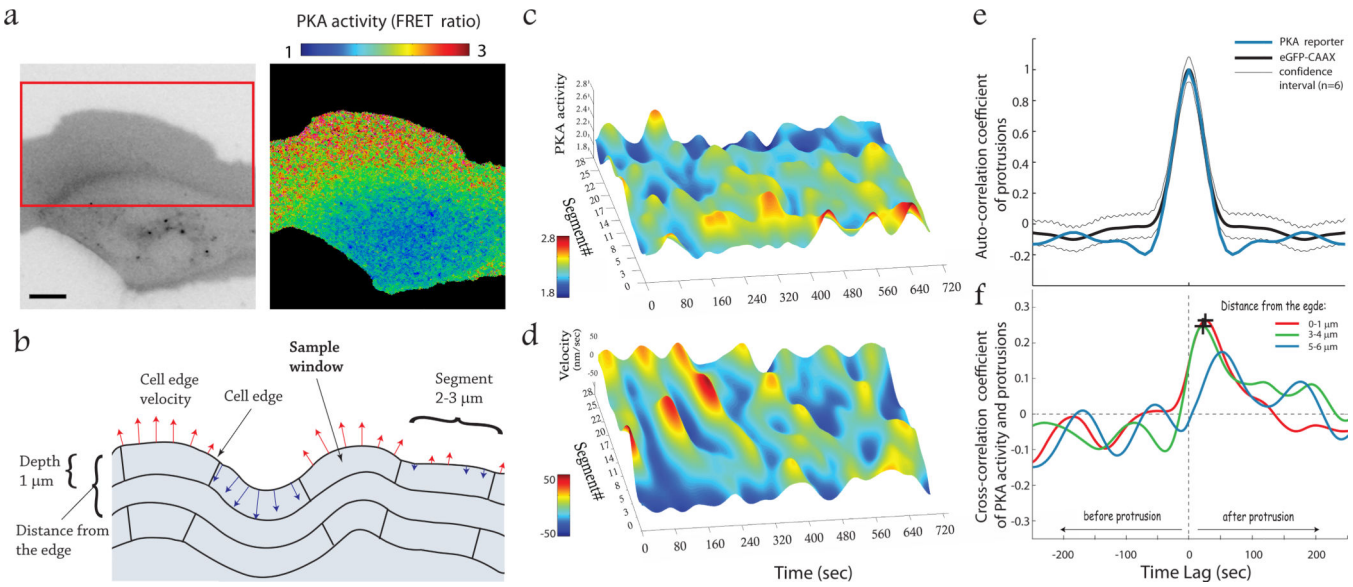

Figure 2. Temporal correlation of PKA activity with cell protrusion

a) Membrane-targeted FRET reporter of PKA activity was used to identify the cell edge (*left*) and to monitor PKA activity (*right*). Red box shows the region that was used for the analysis of PKA activity in protrusions. Scale bar is 10 μm. b) The cell edge was divided into segments of 2–3 μm long in accordance with the length scale of protrusion events (see text). Red and blue vectors correspond to protrusions and retractions, respectively. Cell edge displacements were calculated every 0.6 μm and averaged for each segment. For each segment, a series of consecutive 1μm deep sampling windows were defined with the first window adjacent to the edge. c) PKA activities (color and height) within 1 μm of the cell edge were measured as FRET ratios of pmAKAR3 (range = 1.8 (blue) to 2.8 (red)) at 10 sec intervals over a 720 sec interval for different segments. d) The leading edge position was assessed from cell images taken over 720 sec at 10 sec intervals and was used to calculate the protrusion or retraction velocity (color and height) as a function of time (abscissa) for each segment. Velocity values are color-coded from −50 nm/sec (blue) to 50 nm/sec (red). e) Spline fits representing average temporal autocorrelation of protrusions in a cell expressing the PKA FRET reporter and in control cells (n=7, 4 experiments). f) Spline fits representing temporal cross-correlation between the protrusion velocity and PKA activity at different distances from the cell edge (n=3, 3 experiments). Black crosses show the 95% confidence intervals for the location of cross-correlation peaks.

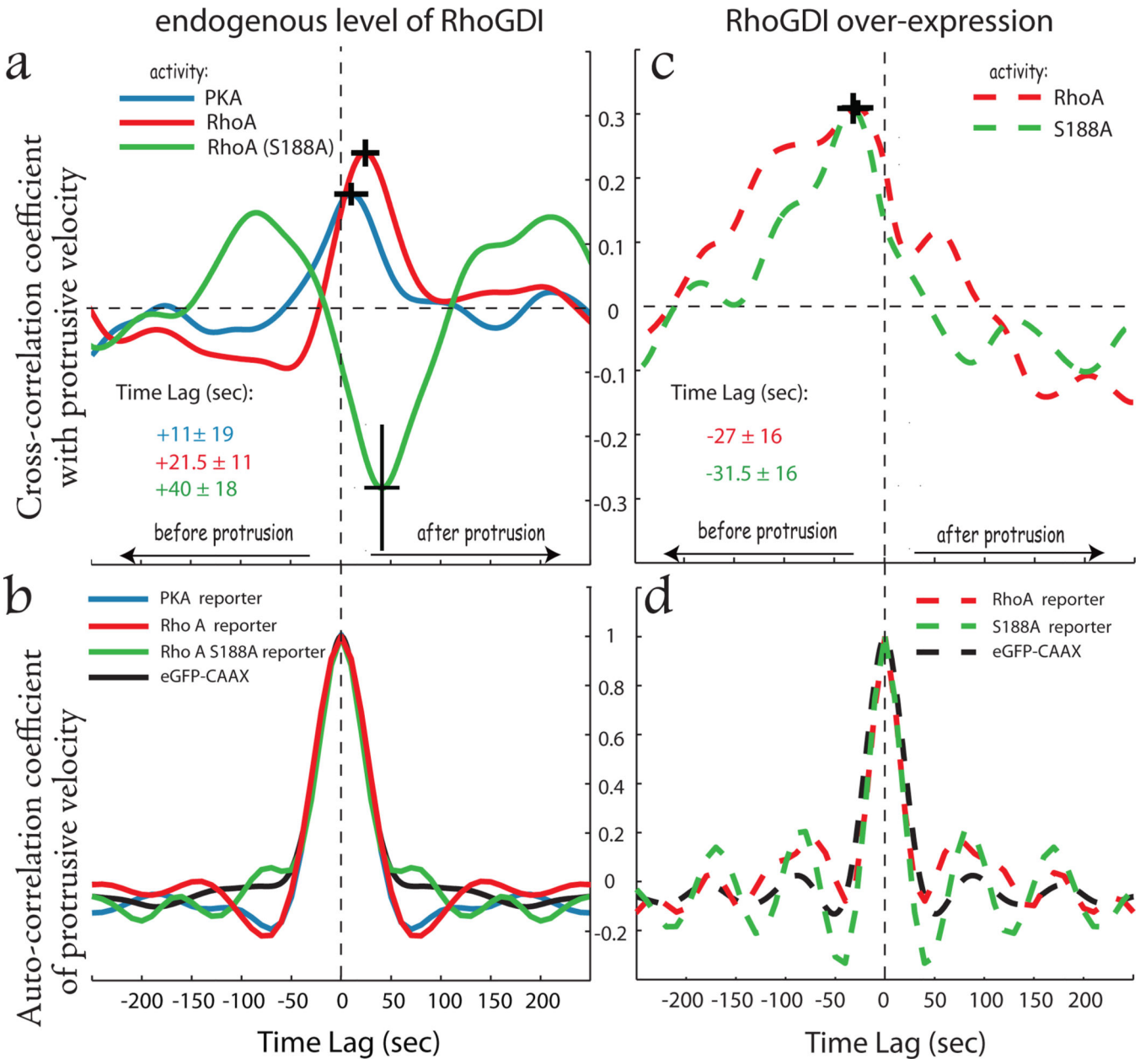

Figure 3. PKA phosphorylation of RhoA regulates the dynamics of RhoA activity at the cell edge

a) Average temporal cross-correlations between the protrusion velocity and activity of various enzymes: PKA (blue line, n=6, 4 experiments), RhoA (red line, n=5, 4 experiments), and RhoA(S188A) mutant (green line, n=4, 3 experiments). Black crosses show the 95% confidence intervals for the strongest correlations (positive or negative). Peak of PKA activity was 12 sec, [CI ±18] after maximal protrusion velocity, whereas peak of RhoA activity occurred 21.5 sec, [CI ±11] after maximal protrusion velocity. RhoA(S188A) activity had a negative correlation with protrusion velocity with a delay of 40 sec, [CI ±18]. b) Temporal cross-correlation of protrusion velocity with RhoA activity in cells co-expressing RhoGDI with RhoA wild type (dashed red line, n=3, 2 exp) or RhoA(S188A) (dashed green line, n=5, 3 experiments) FRET reporters. Note the positive correlation of

maximal activities of both RhoA (−27 sec, [CI ±16] and RhoA(S188A) (−31.5 sec, [CI ±16]) with protrusion velocity. c) Average temporal autocorrelation of protrusion velocity in cells expressing the PKA, RhoA, and RhoA(S188A) activity reporters is compared with cells expressing eGFP-CAAX construct (n=6). d) Average temporal autocorrelation of protrusion velocity in a cell co-expressing RhoGDI with RhoA or RhoA(S188A) activity reporters, in comparison with cells co-expressing RhoGDI with eGFP-CAAX (n=5, 2 experiments).

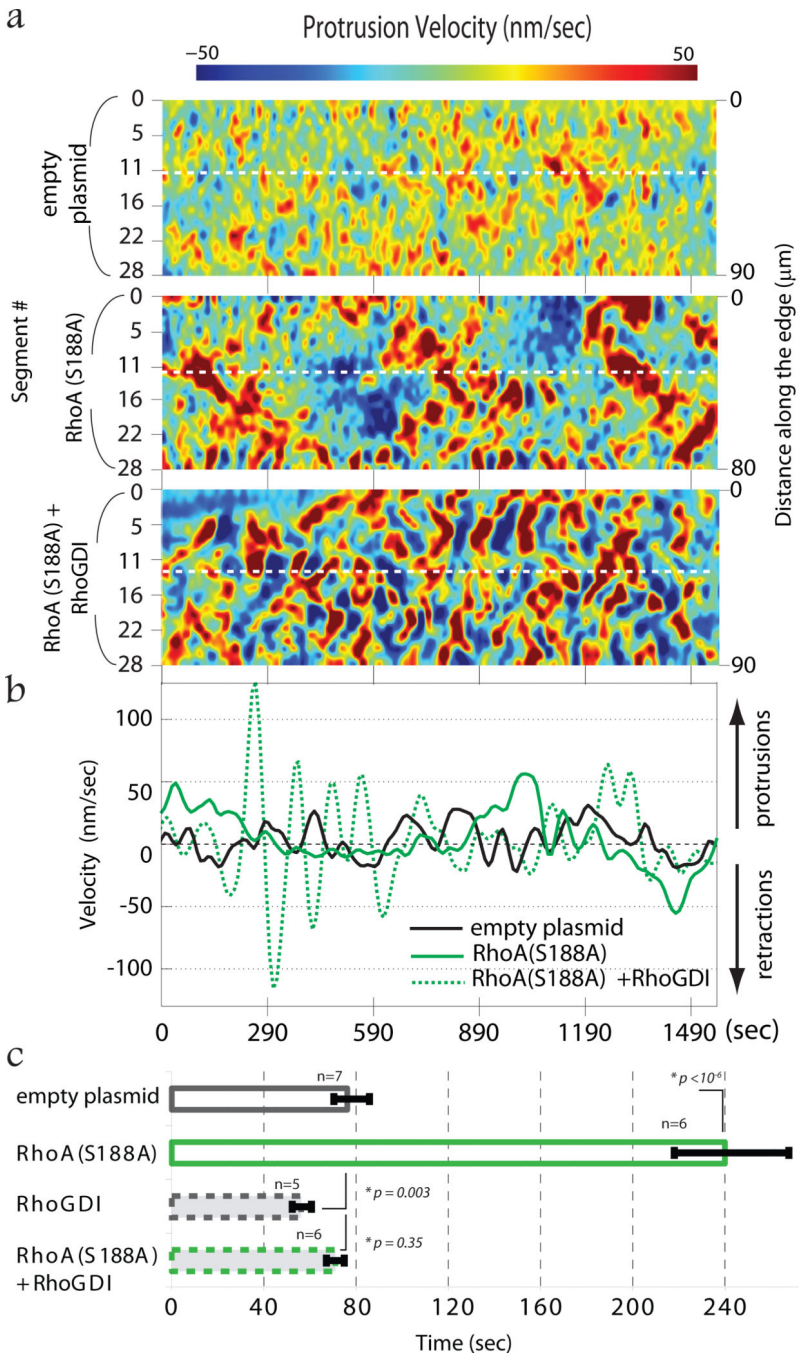

Figure 4. Increased RhoGDI complements the effect of over-expression of RhoA(S188A) on protrusion duration

a) Protrusion-velocity maps of the leading edge of a control cell transfected with empty plasmid and cells over-expressing RhoA(S188A) without and with RhoGDI. The ordinate indicates the edge segment number (left) and the distance along the edge in μm (right). The abscissa indicates time. Velocity values are color-coded from −50 nm/sec (blue) to 50 nm/sec (red). b) Protrusion velocity is plotted against time for the segments indicated by the white dashed lines in (a). c) Duration of protrusions in cells transfected with empty plasmid

(n=7, 4 experiments), cells over-expressing RhoA(S188A) (n=6, 4 experiments), RhoGDI (n=5, 2 experiments), and RhoA(S188A) together with RhoGDI (n=6, 4 experiments).

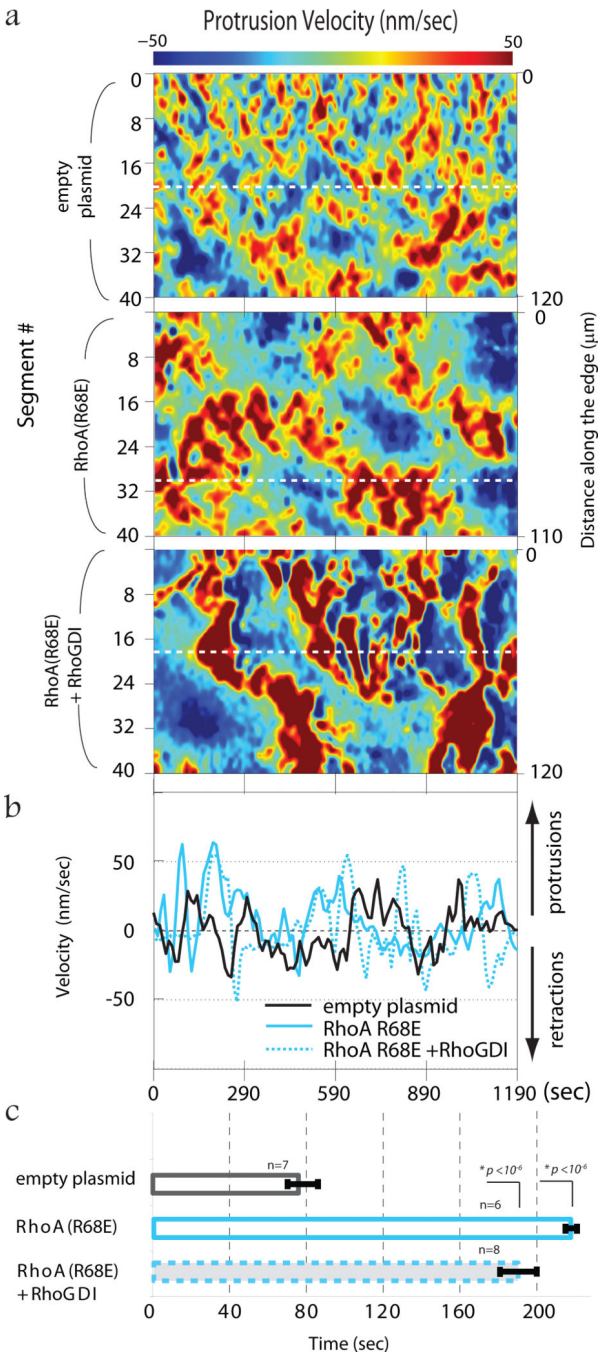

Figure 5. Increased RhoGDI does not complement the effect of over-expression of RhoA(R68E) on protrusion duration

a) Maps of protrusion velocity of the leading edge of a control cell transfected with an empty plasmid and cells over-expressing RhoA(R68E) without and with RhoGDI. The ordinate indicates the edge segment number (left) and the distance along the edge in μm (right). The abscissa indicates time. Velocity values are color-coded from −50 nm/sec (blue) to 50 nm/sec (red). b) Protrusion velocity is plotted against time for the segments indicated by the white dashed lines in (a). c) Duration of protrusions in cells transfected with empty

plasmid (n=7), cell over-expressing RhoA(R68E) (n=6, 3 experiments), and RhoA(R68E) together with RhoGDI (n=8, 4 experiments).

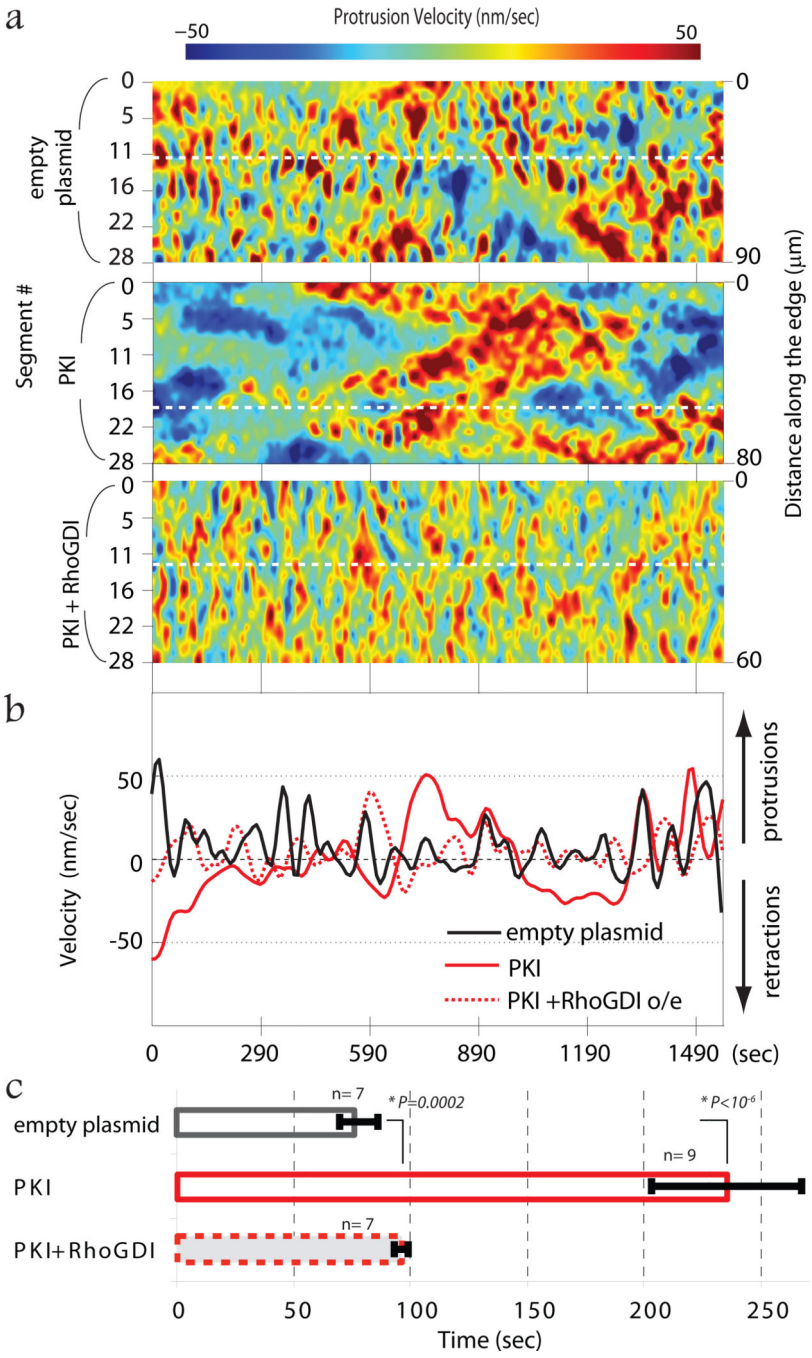

Figure 6. Over-expression of RhoGDI compensates for the effect of PKA inhibition on protrusion morphodynamics

a) Protrusion-velocity maps of the leading edge of a control cell transfected with an empty plasmid and cells over-expressing PKI without and with RhoGDI. The ordinate indicates the edge segment number (left) and the distance along the edge in μm (right). The abscissa indicates time. Velocity values are color-coded from −50 nm/sec (blue) to 50 nm/sec (red). b) Protrusion-retraction velocity plot at the segments indicated by the white dashed lines in (a). c) Duration of protrusions in control cells transfected with empty plasmid (n=7), cells

over-expressing PKI (n=9, 4 experiments), and over-expressing both PKI and RhoGDI (n=7, 4 experiments).

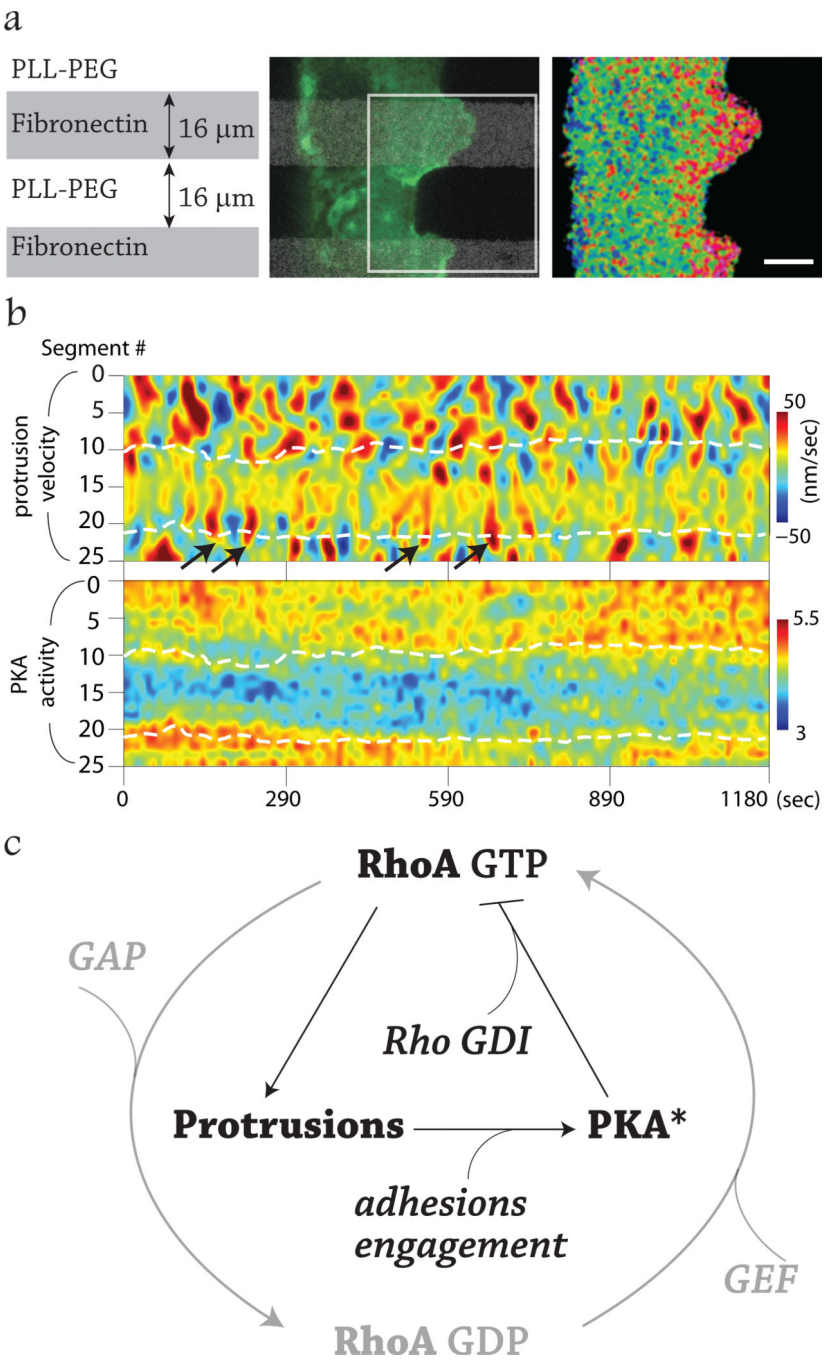

Figure 7. PKA activation requires both protrusion and adhesion of the leading edge to create a self-inhibiting feedback loop

a) PtK1 cell expressing PKA activity reporter were plated on micropatterned substrates, in which 16 μm wide stripes of fibronectin were separated by 16μm stripes of inert polylysine-polyethylene glycol (PLL-PEG). The leftmost panel illustrates the patterning of the stripes as defined by the localization of fluorescently-labeled fibronectin and dotted lines in the middle and right panel show the borders of the stripes. The localization of the FRET probe in the middle panel (green) was used to identify the cell edge in the region outlined by white box. The rightmost panel depicts the PKA activity displayed as a color-coded FRET ratio at

the first time point (range =3 (blue) to 5.5 (red)). Scale bar is 10 μm. b) *Top panel*: a morphodynamic protrusion map of the region in the white box in panel b color-coded from −50 nm/sec (blue) to 50 nm/sec (red). The white dashed lines outline the borders between adhesive (fibronectin) and non-adhesive (PLL-PEG) substrates. Protrusive domains indicated by arrows show the physical continuity of protrusions between the adherent and non-adherent zones. *Bottom panel*: a PKA activity map as FRET ratios of pmAKAR3 (range =3 (blue) to 5.5 (red)) within 1μm from the cell edge. PKA activity is absent in the non-adherent zone. c) PKA, RhoA, and RhoGDI form a protrusion-retraction pacemaker. RhoA activity initiates protrusion of the adherent leading edge resulting in PKA activation. PKA phosphorylates RhoA at Ser188, leading to increased affinity for RhoGDI. RhoGDI binding both removes RhoA from the membrane and interferes with its coupling to effectors resulting in termination of protrusions, thereby completing a self-inhibiting negative feedback loop that acts as a pacemaker of the protrusion-retraction cycle. When PKA is inhibited or RhoA over-expression exceeds available RhoGDI, protrusion duration and amplitude are markedly increased. This much slower cycle suggests the existence of a second slower default pacemaker, such as the RhoA GTP-GDP cycle depicted in light gray.